Implantable microenvironments to attract hematopoietic stem/cancer cells

Jungwoo Lee[a], Matthew Li[a,b], Jack Milwid[a,b], Joshua Dunham[c], Claudio Vinegoni[c], Rostic Gorbatov[c], Yoshiko Iwamoto[c], Fangjing Wang[a], Keyue Shen[a], Kimberley Hatfield[d], Marianne Enger[e], Sahba Shafiee[f], Emmet McCormack[f], Benjamin L. Ebert[g,h], Ralph Weissleder[c], Martin L. Yarmush[a,i], and Biju Parekkadan[a,h,1]

[a]Center for Engineering in Medicine and Surgical Services, Massachusetts General Hospital, Harvard Medical School and Shriners Hospital for Children in Boston, MA 02114; [b]Harvard-MIT Health Sciences and Technology, Cambridge, MA 02139; [c]Center for Systems Biology, Massachusetts General Hospital, Harvard Medical School, Boston, MA 02114; [d]Section of Hematology, Department of Medicine, Haukeland University Hospital, 5021 Bergen, Norway; [e]Gade Institute, University of Bergen, 5020 Bergen, Norway; [f]Department of Hematology, Institute of Internal Medicine, Haukeland University Hospital, University of Bergen, 5020 Bergen, Norway; [g]Department of Hematology, Brigham and Women's Hospital, Harvard Medical School, Boston, MA 02114; [h]The Harvard Stem Cell Institute, Boston, MA 02115; and [i]Department of Biomedical Engineering, Rutgers University, Piscataway, NJ 08854

Edited by Mina J. Bissell, E. O. Lawrence Berkeley National Laboratory, Berkeley, CA, and approved October 22, 2012 (received for review May 21, 2012)

The environments that harbor hematopoietic stem and progenitor cells are critical to explore for a better understanding of hematopoiesis during health and disease. These compartments often are inaccessible for controlled and rapid experimentation, thus limiting studies to the evaluation of conventional cell culture and transgenic animal models. Here we describe the manufacture and image-guided monitoring of an engineered microenvironment with user-defined properties that recruits hematopoietic progenitors into the implant. Using intravital imaging and fluorescence molecular tomography, we show in real time that the cell homing and retention process is efficient and durable for short- and long-term engraftment studies. Our results indicate that bone marrow stromal cells, precoated on the implant, accelerate the formation of new sinusoidal blood vessels with vascular integrity at the microcapillary level that enhances the recruitment hematopoietic progenitor cells to the site. This implantable construct can serve as a tool enabling the study of hematopoiesis.

hydrogel scaffolds | leukemia | mesenchymal stem cells | stem cell niche | tissue engineered bone marrow

Migration and engraftment of hematopoietic stem and progenitor cells (HSPCs) in the bone marrow are widely observed phenomena with many clinical ramifications. In HSPC mobilization, cytokine administration promotes the egress of stem and progenitor cells into the peripheral circulation (1). In HSPC transplantation, cells are transfused into the venous circulation of the recipient and home to the marrow for engraftment (2). Migration and engraftment also are critical in the study of hematopoietic cancers and solid tumor metastasis. Blood and disseminated tumor cells share many similarities with the bone marrow homing and engraftment process of HSPCs (3, 4). Moreover, the bone marrow has emerged as an attractive therapeutic target for cellular and molecular therapies that aim to modulate the host's blood and immune system (5–8). A deeper understanding of the mechanism that governs HSPC trafficking and engraftment is essential to improve the clinical effectiveness of hematopoietic transplantation, the development of new oncotherapies, and the targeting of bone marrow therapeutics.

A major challenge in probing the bone marrow microenvironment is that the experimental platforms to do so are nonphysiological and/or low-throughput in nature. In vitro models using transwell chambers have been explored to understand HSPC migration (9, 10), but these experiments do not account for the complexity of this tissue and its components. The components of the bone marrow niche have been recognized as major regulators of HSPC migration (11–13). These components include (*i*) a specialized sinusoidal vasculature, the gateway of hematopoietic cell trafficking; (*ii*) nonhematopoietic cells that support retention and engraftment by direct cell–cell interactions and by the secretion of soluble and insoluble factors; and (*iii*) a sponge-like geometry that concentrates hematopoietic cells and molecules within the cavity. In vivo experiments using adoptive transfer or parabiotic mouse models retain these components and are the gold standard for studying hematopoietic cell trafficking in a physiological setting (14, 15). Although these methods provide valuable insight into migration and functional engraftment of HSPCs, in situ analysis of the dynamics of cells in the bone marrow remain elusive because of the anatomical inaccessibility and opacity of bone. Intravital imaging of calvarial bone marrow has been developed to capture an unprecedented level of HSPC dynamics in the bone marrow and has contributed significantly to our understanding of hematopoietic niches (16, 17). Aside from the likelihood that calvarial bone may not represent other classical marrow cavities, a key limitation with this approach and other in vivo studies is that the bone marrow microenvironment is determined by the host's genetics with little opportunity for manipulating cell populations in a controlled fashion. These limitations also restrict the modeling of human-specific environmental interactions.

The goal of this study was to build a reproducible and accessible structure that can be used to create localized microenvironments with controlled and defined variables for experimentation. Ectopic implants that recreate key features of a tissue are an intermediate approach that can offer a tremendous advantage to the study and manipulation of a microenvironment for basic and applied research (18). Investigators have attempted to make tissue-engineered structures that resemble bone (19–22), but considerable improvements are needed to allow adoption of these constructs in hematopoietic cell biology. We focused on important design criteria including (*i*) the opportunity for reproducible and user-defined properties such as the choice of substrate, extracellular matrix, cell types, and degradability; (*ii*) the ability to induce sinusoidal and medullar spaces emulating tissue development; (*iii*) accessibility and suitability for high-content imaging and complementary histological/cytological analysis; and, most importantly, (*iv*) the functional ability to capture and retrieve endogenous and transplanted hematopoietic cells efficiently. In this work, we have engineered humanized subcutaneous (s.c.) implants that combine a biomimetic design of hydrogel scaffolds with human bone marrow stromal cells (BMSCs) to form an artificial marrow cavity with high analytic capacity. A polyacrylamide hydrogel was used as the scaffolding material because it is biocompatible, mechanically durable, and amenable to uniform surface chemistry to functionalize

Author contributions: J.L., B.L.E., R.W., M.L.Y., and B.P. designed research; J.L., M.L., J.M., J.D., C.V., R.G., Y.I., F.W., K.S., K.H., M.E., S.S., E.M., and B.P. performed research; E.M., B.L.E., and R.W. contributed new reagents/analytic tools; J.L., E.M., and B.P. analyzed data; and J.L. and B.P. wrote the paper.

The authors declare no conflict of interest.

This article is a PNAS Direct Submission.

[1]To whom correspondence should be addressed. E-mail: biju_parekkadan@hms.harvard.edu.

This article contains supporting information online at www.pnas.org/lookup/suppl/doi:10.1073/pnas.1208384109/-/DCSupplemental.

the material (23). An interesting feature of this implant is that it, in synergy with preseeded BMSCs, attracts and retains endogenous or systemically administered hematopoietic progenitor cells as well as other cells that have tropism for bone marrow (e.g., leukemia cells). The system thus allows systematic investigations of these cell populations in an easily accessible model, using imaging technologies with single-cell resolution.

Results

Microfabricated Hydrogel Scaffolds Mimic the Anatomy of Bone Marrow Extracellular Matrix. Bone marrow is a soft, gelatinous, vascular, and cellular tissue that fills the inner space of bone matrix. Once all cellular and extracellular contents are removed, trabecular bone shows a sponge-like porous structure [pore diameter (D) = 300–900 μm] formed by the assembly of highly oriented type I collagen bundles (Fig. 1*A*). We designed our bioengineered implants to mimic the physical and anatomical features of the bone marrow while retaining a high analytic capacity. We used a template-based fabrication method using colloidal crystals to create polyacrylamide hydrogel scaffolds with precise microstructure that resembles decellularized bone (24–27). The final composition of the scaffold synthesis was a hydrogel that consisted of repeating units of hollowed out "cavities" interconnected by "junctions." The dynamic storage modulus of the hydrogel scaffold was 18.3 ± 6.8 kPa at 5% strain, comparable to that of other soft tissues (28, 29) (Fig. S1). Type I collagen subsequently was conjugated on the scaffold surface at a concentration of 36.46 ng/mL using an intermediate, heterobifunctional crosslinker that displayed amine groups to form peptide bonds. The collagen coating did not alter the overall mechanical property of the scaffold but aided in future cell-adhesion studies. Scanning electron microscopy revealed remarkable structural similarity between the scaffold and decellularized cancellous bone at the microscopic and submicroscopic levels (Fig. 1*B*).

3D Culture of Human BMSCs Enhances Release of Secreted Factors. BMSCs are key support cells that nurture HSPCs and are considered to be regulators of the bone marrow (30, 31). We hypothesized that BMSC scaffolds might provide a more physiological microenvironment to attract and organize hematopoietic cells. BMSCs were isolated from healthy human bone marrow aspirates and were expanded ex vivo. BMSCs were $CD44^+$, $CD106^+$, $CD14^-$, $CD34^-$, $CD45^-$, $CD73^+$, and $CD105^+$ and retained the ability to differentiate into osteogenic and adipogenic cells, consistent with their multipotent phenotype (32). Human BMSCs adhered to the collagen-coated hydrogel surface as a stromal feeder layer with remarkable uniformity (Fig. 1*C*).

We envisioned that, for the implant to create a local concentrated chemical environment for hematopoiesis to take place outside the bone marrow, the factors secreted by BMSCs (33) within the scaffold had to be optimized as a function of biomaterial pore size (Fig. 1*D*). The pore size of the material is a combination of the cavity size and the junction size, which scales by a factor of approximately one-fourth the diameter of the cavity. For clarity, we refer to changes in pore size as a reflection of the change in cavity size. BMSC seeding and the release of secreted factors from the scaffold were compared in a range of cavity sizes to identify an optimum microenvironment. The homogeneity of BMSC coating correlated linearly with pore size but correlated inversely with seeding efficiency. For example, the smaller-cavity scaffolds (D = 75–105 μm) showed almost 90% BMSC-loading efficiency, but the seeding quality was compromised with a cellular gradient and local aggregation. The larger-cavity scaffolds (D = 425–500 μm) exhibited homogenous cell distribution across the scaffold but lost about 50% of cells (Fig. 1*E* and Fig. S2). We next collectively evaluated BMSC secretions using an in vitro potency assay that quantifies the known paracrine, anti-inflammatory effects of BMSCs on immune cells (34). BMSC-conditioned medium collected from the biomaterials had enhanced anti-inflammatory effects (less IFN-γ release by stimulated immune cells) with reducing cavity size as compared with 2D culture platforms (Fig. 1*F*). These data indicate a significant enhancement of the potency of BMSC-secreted factors by 3D hydrogel culture; this enhancement could be caused by a global up-regulation of particular agents or new mediators that were expressed in 3D. We also measured a subset of known BMSC-secreted factors that are associated with bone marrow homeostasis. BMSC secretion of VEGF, IL-6, and IL-8 was enhanced in these 3D biomaterials, whereas secretion of

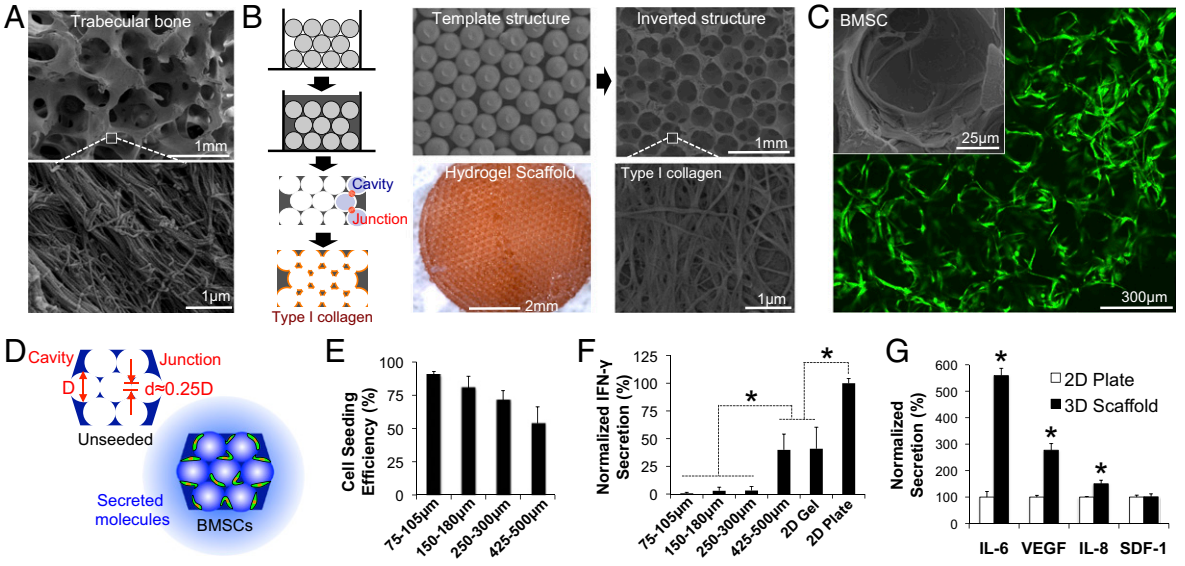

Fig. 1. Biomimetic design of 3D microfabricated scaffolds and human BMSC culture. (*A*) Scanning electron microscopic images of demineralized bovine cancellous bone at different magnifications. (*B*) Fabrication scheme with scanning electron microscopy and camera images at corresponding stages. (*C*) Scanning electron microscopic and reconstructed 3D confocal images of human BMSC coatings in the scaffold. (*D*) Representation of the local chemical environment created by BMSCs. (*E*) Efficiency of cell seeding is dependent on cavity size. (*F*) Normalized IFN-γ secretion of human peripheral blood mononuclear cells with BMSC-conditioned medium and lipopolysaccharide relative to the highest overall value. (*G*) Comparison of secretion of specific soluble factors by BMSC cultures on a 2D plate and 3D scaffold (D = 150–300 μm). $*P < 0.05$.

stem cell-derived factor-1 (SDF-1) was independent of culture formats (Fig. 1*G*). Because of these results, we chose a cavity size of 150–300 μm for in vivo testing to allow maximum space for host cell infiltration/migration in the scaffold without compromising BMSC seeding efficiency, homogeneity, and function.

Subcutaneously Implanted BMSC Scaffolds Induce Vascularized, Hematopoietic Tissue Formation. We developed and optimized an implantation method to observe the effects of scaffolds on the native hematopoietic system in recipient mice. Immunocompromised mice were s.c. implanted with human BMSC-seeded or unseeded scaffolds having four different cavity diameters. The effect of BMSCs on scaffold cell infiltration was dependent on cavity size in a distinct range of 150–300 μm (Fig. S3). Semiquantitative histological analysis of this cavity range showed rapid increment of nucleated cell infiltration in BMSC-seeded scaffolds compared with unseeded scaffolds over a 4-wk period (Fig. S4). These data correlate well with previous in vitro characterization and confirmed that scaffolds with a cavity of 150–300 μm were optimal for BMSC-mediated tissue formation in vivo.

We next characterized the interscaffold vasculature development of implanted biomaterials. Four weeks after implantation, BMSC implants grossly showed pronounced high-bore vessel formation that presumably perfused the newly formed microtissue (Fig. 2*A*). Corrosion casts of the biomaterials verified patent macroscopic vasculature that gradually extended throughout the entire structure (Fig. 2*B*). Immunohistostaining of mouse CD31, a marker found primarily on endothelial cells, was significantly higher in BMSC-seeded scaffolds and was consistent with increased angiogenesis (Fig. 2 *C* and *D*). VEGF receptor 3 (VEGFR3), a specific receptor expressed by sinusoidal endothelium (35), also was detected in all scaffolds, suggesting that a specialized endothelial cell structure was induced by the biomaterial (Fig. 2*E*). We further examined the interscaffold vascularization process by surgically grafting a dorsal window chamber directly on to the implanted scaffold for intravital microscopy (Fig. 2*F*). Intravenously (i.v.) injected FITC-dextran illuminated the vasculature through the transparent hydrogel matrix and substantiated real-time blood circulation in these microenvironments. Hematopoietic cells residing within the material exhibited autofluorescence at 620–680 nm (Fig. S5), which helped to distinguish these cells from the implant. In general, the diameter of recruited blood vessels decreases gradually as they enter the scaffolds but remains similar within the scaffolds, akin to arteriolar perfusion of a capillary bed (Fig. 2*G*). Notably, more than 70% of interscaffold blood vessels have diameters between 10 and 50 μm, values that are comparable with the known sinusoidal diameters of human bone marrow (36) (Fig. 2*H*).

The implanted biomaterials had an organized and distinct cellular milieu in BMSC-seeded scaffolds as compared with unseeded controls. Unseeded scaffolds generally contained a mixture of fibroblastic and adipocytic cells, whereas BMSC-seeded scaffolds were populated with atypical hematopoietic cells that had a high nuclear:cytoplasm ratio consistent with the morphology of progenitor cells (Fig. 2*I*). By overlaying corrosion casts and histological and scanning electron microscopy images, the tissue architecture in the scaffolds could be compartmentalized into three distinct regions: (*i*) blood vessels located at the cavity center, (*ii*) intermediate, nonhematopoietic tissue, and (*iii*) a cortical region harboring hematopoietic cells (Fig. 2*J* and Fig. S6). The estimated tissue space created by a single scaffold was equivalent to 2% of the endogenous mouse bone marrow or 0.04% total body weight (Fig. S7).

BMSC Scaffolds Attract Endogenous Hematopoietic Progenitors to the Implantation Site. Four weeks after implantation, we harvested hematopoietic cells from the retrieved scaffolds and evaluated the identity of cells. BMSC-laden scaffolds (0.68 ± 0.21%) were more than a log-enriched in $Lin^{-}Sca\text{-}1^{+}c\text{-}kit^{+}$ (LSK) progenitor cells as compared with unseeded scaffolds (0.05 ± 0.03%) (Fig. 3*A*). This recruitment was specific to BMSCs, because scaffolds seeded with human skin fibroblasts did not attract the same percentage of LSK cells and had calcification associated with the material (Figs. S8 and 9). The frequency of LSK cells in BMSC-seeded scaffolds was ~20% of the endogenous bone marrow after normalizing for cell number (Fig. 3*B*). No major differences were observed in hematopoietic lineage cells in the implants except for higher frequencies of $CD3^{+}$

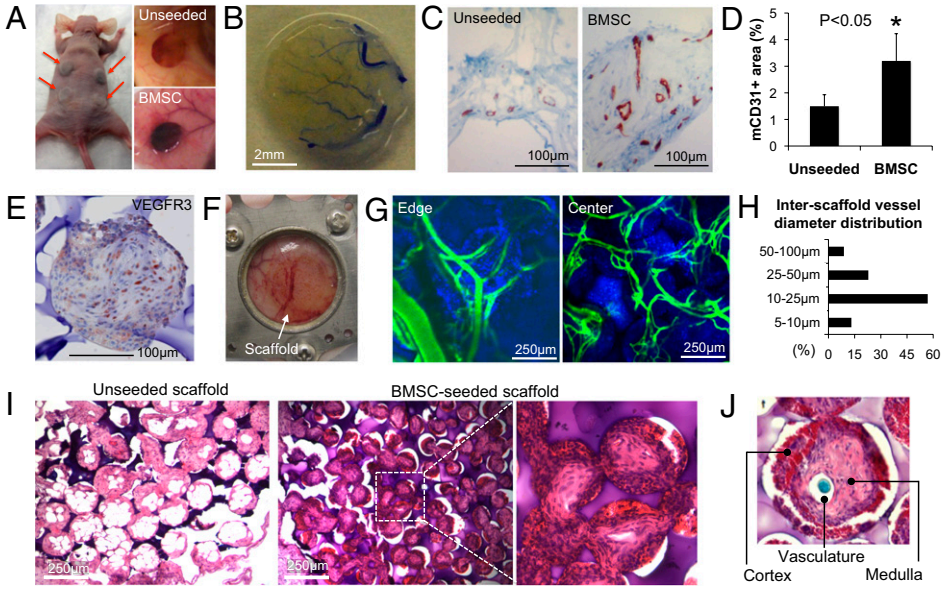

Fig. 2. Development of vascularized, extramedullary marrow tissue. (*A*) Gross histological observations 4 wk after implantation show increased vascularization in BMSC-seeded scaffolds. (*B*) Optical image of corrosion-casted and decellularized BMSC-seeded scaffold. (*C*) Immunostaining of $mCD31^{+}$ endothelial cells. (*D*) Quantitative comparison of $mCD31^{+}$ area 4 wk after implantation showing significant increase by BMSCs. (*E*) Immunohistostaining of mVEGFR3 in BMSC-seeded scaffolds. (*F*) Dorsal window chamber grafted on top of the implanted scaffold. (*G*) Intravital imaging of interscaffold vasculature (green, blood vessels; blue, autofluorescent for contrast). (*H*) Distribution of interscaffold vessel diameters. (*I*) Histological comparison of H&E-stained tissue sections from unseeded and BMSC-seeded scaffolds. (*J*) Interscaffold tissue compartment model.

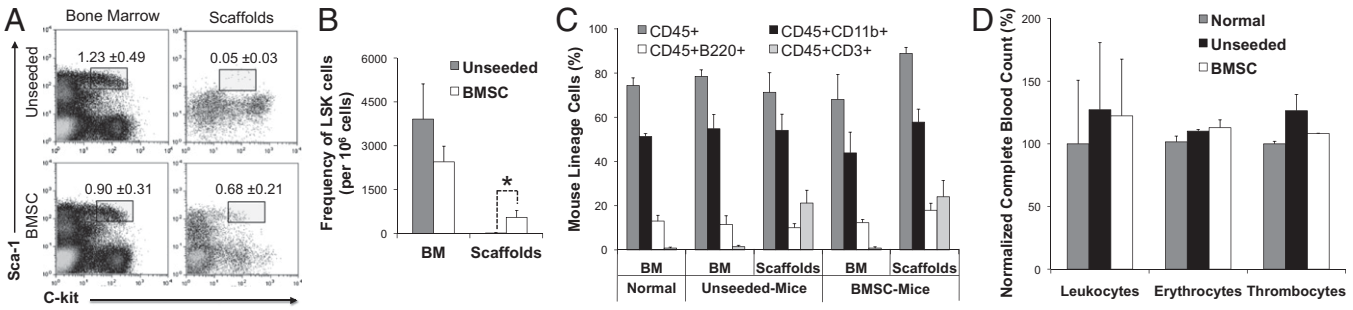

Fig. 3. Local and systemic hematopoietic cell analysis 4 wk after scaffold implantation. (*A*) Detection of LSK cells by flow cytometry from explanted scaffolds and endogenous bone marrow cells ($n = 4$) and (*B*) their frequency (*$P < 0.05$). BM, bone marrow. (*C*) Comparison of linage cell analyses in the bone marrow and scaffold cells. (*D*) Normalized complete peripheral blood count of scaffold-implanted mice with respect to normal mice.

cells, which were independent of BMSCs (Fig. 3*C*). In addition, no systemic differences were observed in blood cells of scaffold-implanted mice (Fig. 3*D*). Collectively, these data suggest that these implants can attract endogenous mouse LSK cells spontaneously and develop an equilibrium state with the native bone marrow that does not alter overall blood cell counts.

Retention of Human Hematopoietic Progenitor Cells After Direct Delivery to BMSC Scaffolds. We used a direct injection procedure to examine whether the scaffold can accommodate and subsequently detain a large number of hematopoietic cells (Fig. 4*A*). Approximately 5×10^5 human CD34$^+$ cells that were prestained with an infrared dye were injected directly into a scaffold in sublethally irradiated mice. We monitored the cells' short-term retention within the scaffolds for 3 d using fluorescent molecular tomography (FMT). FMT revealed that a higher portion of human CD34$^+$ cells remained in the BMSC-laden scaffolds than in unseeded scaffolds, whereas the fluorescent signal decreased rapidly in mice without scaffolds that received an s.c. cell injection (Fig. 4*B*). Immunohistological analysis after 7 d showed significantly increased cellularity within the scaffolds, indicating successful transplantation of mononuclear cells into the scaffolds (Fig. S10).

We further evaluated long-term engraftment of directly transplanted human CD34$^+$ HSPCs (2×10^5) to the scaffolds of sublethally irradiated NOD-*scid* IL2rγ^{null} (NSG) mice. Mice without scaffolds served as controls and were injected i.v. or s.c.. After 16 wk human CD45$^+$ leukocytes were detected in the scaffolds and also in the native bone marrow. BMSC-seeded scaffolds retained a significantly higher percentage of human CD45$^+$ cells than unseeded scaffolds (Fig. 4*C*). The bone marrow of both BMSC and unseeded scaffolds showed significantly higher percentages of human CD45$^+$ cells than s.c. injected control mice. Although scaffold-implanted mice never reached the levels of human chimerism observed in i.v. recipients of HSPCs, these data show that human cells remain viable for long-term functional studies.

Systemic Recruitment of Intravenously Injected Human HSPCs and Leukemic Cells to Implanted Microenvironments. The value of these implants in recruiting i.v. delivered human HSPCs and leukemic cells was explored next (Fig. 5*A*). Four weeks after implantation, Nu/Nu mice were sublethally irradiated and i.v. injected with 1×10^5 human CD34$^+$ cells. After 3 d, immunohistostaining of human nuclei revealed that implanted scaffolds supported the homing and retention of circulating human CD34$^+$ cells (Fig. 5*B*). We repeated this short-term migration study using fluorescently labeled human TF-1a cells, a model leukemic stem cell line (2×10^6 cells per mouse). Direct confocal imaging of explanted scaffolds shows that significantly more leukemic cells engrafted in BMSC-seeded scaffolds 6 h after injection (Fig. 5*C*). FACS analysis confirmed that there were twice as many TF-1a cells in BMSC-seeded scaffolds than in unseeded scaffolds and that was 39% of TF-1a cells detected relative to the bone marrow engrafted TF-1a cells. (Fig. 5*D*).

We then investigated dynamic interactions between scaffold-induced vasculature and human TF-1a leukemic cells by intravital confocal imaging. Human TF-1a leukemic cells were i.v. injected into implant-bearing mice (2×10^6 cells per mouse). Circulating TF-1a cells were detected 30 min after injection, and their tethering to vessels was noticed after 3 h. TF-1a cells were detected in blank scaffolds (Fig. 5*E* and Movie S1), but significantly more TF-1a cells were engrafted in BMSC-seeded scaffolds (Fig. 5*F* and Movie S2). By 5 h, we began to observe actual extravasation of cells into the scaffold and migration toward the cortical space at single-cell resolution. Further quantitative analysis of vascularly tethered TF-1a cells in the BMSC-seeded scaffold indicated that 75% of circulating leukemic cells tethered

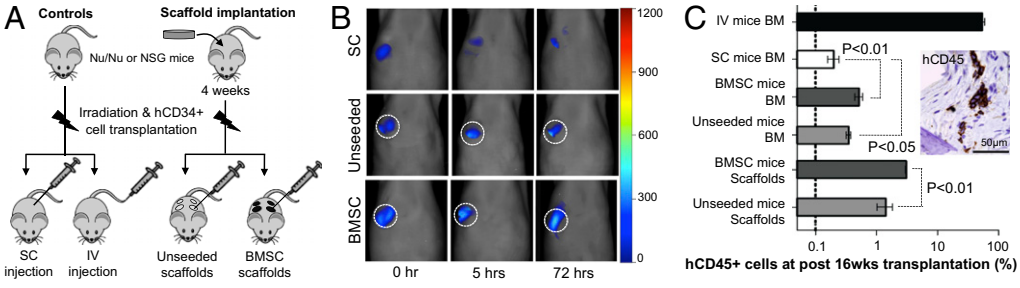

Fig. 4. Retention and engraftment of directly transplanted human bone marrow CD34$^+$ hematopoietic progenitor cells. (*A*) Schematic of experimental design of human CD34+ cell transplantation s.c., i.v., or via implant in sublethally irradiated mice. (*B*) FMT images of 5×10^5 directly injected human CD34$^+$ cells prestained with a near-infrared dye over 3 d show longer retention of HSPCs in BMSC-seeded scaffolds. (*C*) Analysis of human CD45$^+$ cells from endogenous bone marrow and implanted scaffolds 16 wk after transplantation of human CD34$^+$ cells ($n = 4$). Two independent trials were performed. (*Inset*) Immunohistostaining of human CD45$^+$ cells in BMSC-seeded scaffolds.

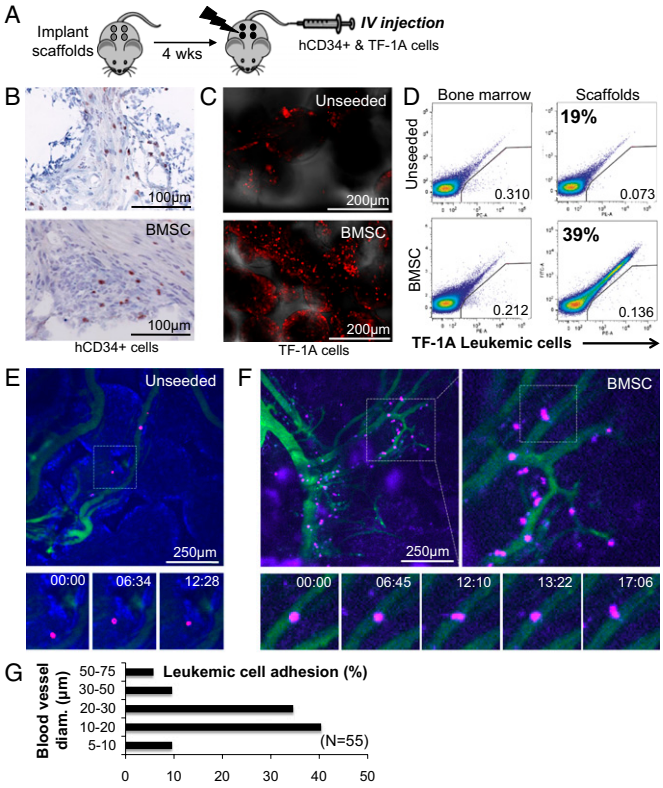

Fig. 5. Homing of i.v. transplanted human bone marrow cells. (*A*) Schematic of experimental design. (*B*) Immunostaining of human nuclei in unseeded and BMSC-seeded scaffolds 3 d after i.v. injection. (*C*) Confocal images of explanted scaffolds 3 d after i.v. injection of prestained TF-1a cells. (*D*) Cytofluorimetry of prestained TF-1a cells from the bone marrow and explanted scaffolds. (*E* and *F*) Intravital confocal image of (*E*) unseeded and (*F*) BMSC-seeded scaffolds 5 h after i.v. injection. (*G*) Correlation between blood vessel diameters and number of adhered leukemic cells.

on interscaffold vasculature having a diameter of 10–30 μm (Fig. 5*G*). These length and time scales of engraftment are highly corroborated by in vivo engraftment of hematopoietic cells and fulfill our biomimetic design goals. These data demonstrate that BMSC-seeded scaffolds could serve as a controlled microenvironment for the study of crosstalk between a tissue and hematopoietic stem and cancer cells.

Discussion

We have developed an implantable microenvironment to enable the detailed and controlled study of bone marrow migration and engraftment of human HSPCs and leukemic cells. The rationale of our approach was inspired by extramedullary hematopoiesis in which the body develops hematopoietic-inductive spaces for the ectopic growth of HSPCs during states of bone marrow failure. This compensatory process is a well-recognized clinical observation that occurs in a variety of nonosseous tissues including the spleen, liver, and skin (37–39). Although extramedullary sites do not have the same microenvironment as the endogenous bone marrow, they are assumed to retain the essential elements involved in HSPC migration and engraftment. We used a bioengineering approach to recapitulate this functional microenvironment s.c. to study hematopoietic biology.

The biomimetic design and analytical capacity of this implant are important aspects that help standardize experimentation (40, 41). For instance, the structure and chemistry of the polyacrylamide hydrogel scaffolds are precise and promote reproducible tissue development after implantation. At a study end point, the hydrogel matrix can be ruptured physically to retrieve cells from the explanted scaffolds for molecular analysis. The optical transparency of hydrogel scaffolds permits high-resolution intravital confocal imaging that is difficult to achieve with conventional engineered bone–tissue scaffolds that typically are made with tricalcium phosphate, hydroxyapatite, and other opaque polymeric materials. These features allow quantitative characterization of this system when combined with conventional analytical methods.

The 3D culture of human BMSCs in hydrogel scaffolds enhanced the secreting function of stromal cells. Interestingly, only specific cytokines were up-regulated in the scaffolds. IL-6, an immunomodulatory cytokine, and VEGF, an angiogenic growth factor, showed dramatically increased levels, whereas IL-8, a chemokine, showed minimal increase. SDF-1 secretion, a separate chemokine pathway, was independent of culture substrates. A 3D geometry built with the hydrogel matrix specifically activated the BMSC secretion pathway, likely by mechanical signaling, and potentially can tailor the secretome of these cells for distinct functions. We presume that the factors secreted by BMSC that are concentrated and released in this environment enhanced the vascularization and attraction of hematopoietic cells that resided with the implant. A significant increase in the number of endogenous HSPCs was detected in BMSC-seeded scaffolds, suggesting that these implanted microenvironments retain some elements of a hematopoietic-inductive milieu, although a detailed analysis of the mechanism is required. Next-generation technology that builds on this platform, including the use of growth factor-impregnated scaffolds, new preseeded cell mixtures that enhance tissue development, and genetically engineered cell types to evaluate competitive engraftment in the same host, can assist in defining a mechanism.

Subdermally implanted scaffolds induced the development of two important tissue structures found in the bone marrow niche: a sinusoidal-like vasculature and interstitial space for the housing of a large number of hematopoietic cells. Previous studies of similar scaffold designs have shown that the pores 30–40 μm in diameter efficiently promote vascularization upon implantation (42). These designs, although promoting vasculature, do not create a separate organized hematopoietic cavity for the influx and efflux of cells. VEGFR3$^+$ endothelium was detected in these materials, indicating that endothelial cells either trafficked to or differentiated at the interface between the biomaterial and the intercavity tissue. The platform can be used to study the interaction of hematopoietic cells with this sinusoidal endothelial structure.

Grafting a skin window to an implant allows direct real-time characterization of the interaction between an implanted microenvironment and trafficking cells at single-cell resolution under physiological conditions. Dorsal skinfold chambers have been used extensively for intravital imaging of tumors and other tissues (43–45); in our study we used this system for in situ observation of hematopoietic cell trafficking in an implanted scaffold. One advantage of a skinfold window chamber is the opportunity to image the microenvironment noninvasively over time scales that are relevant to cell homing, localization, and interactions of hematopoietic stem and cancer cells; currently, the use of other methods for such imaging is limited (46). Our intravital imaging studies demonstrate that (*i*) leukemic cell homing and localization processes occur within 5 h after systemic administration; (*ii*) extravasation requires prevascular adhesion and takes about 20 min; and (*iii*) extravasated leukemic cells actively migrate and localize in the medullary space of the microenvironment. The majority of leukemic cells adhered to blood vessels having diameters of 10–30 μm, two to three times larger than the size of the cells. Our data indicate that the degree of vascularization, vasculature anatomy, and blood flow mechanics may play important roles in leukemic cell migration.

In conclusion, we have demonstrated the potential of an implantable microenvironment for the study of dynamic interactions of hematopoietic stem and cancer cells during engraftment and retention. We envision that such an ectopic marrow system can serve as a clinical research tool that may enable mechanistic

studies of HSPC homing biology as well as intermediate-risk acute myeloid leukemia and myelodysplastic syndrome cell engraftment (which rarely occurs in immunocompromised mice) by improving the efficiency of cell transplantation. Continued advances in these bioengineered implants with newer features to mirror the bone marrow niche can contribute greatly to an understanding of human hematopoietic cell biology.

Materials and Methods

Fabrication of Inverted Colloidal Crystal Hydrogel Scaffolds and Human BMSC Culture. Scaffolds were prepared as described previously (26), and the surface was coated with type I collagen using an amine-reactive cross-linker (Sulfo-SANPAH; Pierce). BMSCs were isolated and expanded as reported previously (32). A dense suspension of BMSCs ($1–5 \times 10^5$ cells in 20–30 μL) was dropped on top of a dehydrated scaffold. After 4–6 h, BMSCs adhered to the pore surface.

Subcutaneous Implantation of Biomaterials in Mice. Athymic Nu/Nu or NOD-*scid* IL2rγ^{null} mice (6–8 wk old) were anesthetized, and a 4-mm incision was made at four different sites to create an s.c. pocket for implantation. Before implantation, BMSCs were cultured within the scaffolds for 1–3 d. All animal experiments were approved by the Institutional Animal Care and Use Committee of Massachusetts General Hospital and the Norwegian Animal Research Authority.

Human Bone Marrow Cell Transplantation. Mice were irradiated sublethally 1 d before cell transplantation. Then 200 μL of human CD34$^+$ cells (1×10^5) or TF-1a leukemic cells (2×10^6) was injected through the tail vein. For direct scaffold or s.c. injection, the injection volume was maintained at 50 μL per scaffold, but cell numbers were varied to match the total number of transplanted cells in i.v. injected mice.

Intravital Confocal Imaging. A dorsal skinfold chamber was installed on top of the implanted scaffold in mice. The mouse was placed on a stage and was imaged using confocal microscopy (Olympus IV100). The target region was found by visualizing the colocalization of autofluorescent hematopoietic cells (emission: 670 nm) with the local vasculature after a tail-vein injection of 10 mg/mL FITC-dextran (excitation: 488 nm/emission: 520 nm). Then $2–3 \times 10^6$ human leukemia cells prestained with a DM-Dil CellTracker dye (Invitrogen) (excitation: 553 nm/emission: 570 nm) were injected followed by real-time confocal imaging of the target region for 30 min every 1–2 h for the first 6 h.

ACKNOWLEDGMENTS. We thank Drs. Peter Miller and Ann Mullally for assistance with flow cytometry; Mihaela Popa and Lene M. Vikebø for technical assistance in animal work; and Peter Waterman for assistance in fluorescent molecular tomography analysis. This work was supported by National Institutes of Health Grants R01EB012521 and K01DK087770, by the Bergen Research Foundation and the Norwegian Cancer Society, by postdoctoral fellowships from the Shriners Hospitals for Children, and by National Cancer Institute Grant 1K99CA163671-01A1.

1. Greenbaum AM, Link DC (2011) Mechanisms of G-CSF-mediated hematopoietic stem and progenitor mobilization. *Leukemia* 25(2):211–217.
2. Copelan EA (2006) Hematopoietic stem-cell transplantation. *N Engl J Med* 354(17): 1813–1826.
3. Shiozawa Y, et al. (2011) Human prostate cancer metastases target the hematopoietic stem cell niche to establish footholds in mouse bone marrow. *J Clin Invest* 121(4): 1298–1312.
4. Colmone A, et al. (2008) Leukemic cells create bone marrow niches that disrupt the behavior of normal hematopoietic progenitor cells. *Science* 322(5909):1861–1865.
5. Adams GB, et al. (2007) Therapeutic targeting of a stem cell niche. *Nat Biotechnol* 25 (2):238–243.
6. Parekkadan B, Milwid JM (2010) Mesenchymal stem cells as therapeutics. *Annu Rev Biomed Eng* 12:87–117.
7. Wagers AJ (2012) The stem cell niche in regenerative medicine. *Cell Stem Cell* 10(4): 362–369.
8. Mikkola HK, Radu CG, Witte ON (2010) Targeting leukemia stem cells. *Nat Biotechnol* 28(3):237–238.
9. Jordà MA, et al. (2002) Hematopoietic cells expressing the peripheral cannabinoid receptor migrate in response to the endocannabinoid 2-arachidonoylglycerol. *Blood* 99(8):2786–2793.
10. Kim CH, Broxmeyer HE (1998) In vitro behavior of hematopoietic progenitor cells under the influence of chemoattractants: Stromal cell-derived factor-1, steel factor, and the bone marrow environment. *Blood* 91(1):100–110.
11. Wilson A, Trumpp A (2006) Bone-marrow haematopoietic-stem-cell niches. *Nat Rev Immunol* 6(2):93–106.
12. Lapidot T, Dar A, Kollet O (2005) How do stem cells find their way home? *Blood* 106(6):1901–1910.
13. Kiel MJ, Morrison SJ (2008) Uncertainty in the niches that maintain haematopoietic stem cells. *Nat Rev Immunol* 8(4):290–301.
14. Wright DE, Wagers AJ, Gulati AP, Johnson FL, Weissman IL (2001) Physiological migration of hematopoietic stem and progenitor cells. *Science* 294(5548):1933–1936.
15. Purton LE, Scadden DT (2007) Limiting factors in murine hematopoietic stem cell assays. *Cell Stem Cell* 1(3):263–270.
16. Sipkins DA, et al. (2005) In vivo imaging of specialized bone marrow endothelial microdomains for tumour engraftment. *Nature* 435(7044):969–973.
17. Lo Celso C, et al. (2009) Live-animal tracking of individual haematopoietic stem/progenitor cells in their niche. *Nature* 457(7225):92–96.
18. Chen AA, et al. (2011) Humanized mice with ectopic artificial liver tissues. *Proc Natl Acad Sci USA* 108(29):11842–11847.
19. Krebsbach PH, et al. (1997) Bone formation in vivo: Comparison of osteogenesis by transplanted mouse and human marrow stromal fibroblasts. *Transplantation* 63(8): 1059–1069.
20. Sacchetti B, et al. (2007) Self-renewing osteoprogenitors in bone marrow sinusoids can organize a hematopoietic microenvironment. *Cell* 131(2):324–336.
21. Song J, et al. (2010) An in vivo model to study and manipulate the hematopoietic stem cell niche. *Blood* 115(13):2592–2600.
22. Tsigkou O, et al. (2010) Engineered vascularized bone grafts. *Proc Natl Acad Sci USA* 107(8):3311–3316.
23. Pelham RJ, Jr., Wang Y (1997) Cell locomotion and focal adhesions are regulated by substrate flexibility. *Proc Natl Acad Sci USA* 94(25):13661–13665.
24. Kotov NA, et al. (2004) Inverted colloidal crystals as three-dimensional cell scaffolds. *Langmuir* 20(19):7887–7892.
25. Lee J, Shanbhag S, Kotov N (2006) Inverted colloidal crystals as three-dimensional microenvironments for cellular co-cultures. *Journal of Materials Chemistry* 16(35): 3558–3564.
26. Lee J, Kotov NA (2009) Notch ligand presenting acellular 3D microenvironments for ex vivo human hematopoietic stem-cell culture made by layer-by-layer assembly. *Small* 5(9):1008–1013.
27. Nichols JE, et al. (2009) In vitro analog of human bone marrow from 3D scaffolds with biomimetic inverted colloidal crystal geometry. *Biomaterials* 30(6):1071–1079.
28. Levental I, Georges PC, Janmey PA (2007) Soft biological materials and their impact on cell function. *Soft Matter* 3(3):299–306.
29. Krouskop TA, Wheeler TM, Kallel F, Garra BS, Hall T (1998) Elastic moduli of breast and prostate tissues under compression. *Ultrason Imaging* 20(4):260–274.
30. Dazzi F, Ramasamy R, Glennie S, Jones SP, Roberts I (2006) The role of mesenchymal stem cells in haemopoiesis. *Blood Rev* 20(3):161–171.
31. Prockop DJ, Kota DJ, Bazhanov N, Reger RL (2010) Evolving paradigms for repair of tissues by adult stem/progenitor cells (MSCs). *J Cell Mol Med* 14(9):2190–2199.
32. Parekkadan B, et al. (2007) Mesenchymal stem cell-derived molecules reverse fulminant hepatic failure. *PLoS ONE* 2(9):e941.
33. Pittenger M (2009) Sleuthing the source of regeneration by MSCs. *Cell Stem Cell* 5(1): 8–10.
34. Jiao J, Milwid JM, Yarmush ML, Parekkadan B (2011) A mesenchymal stem cell potency assay. *Methods Mol Biol* 677:221–231.
35. Hooper AT, et al. (2009) Engraftment and reconstitution of hematopoiesis is dependent on VEGFR2-mediated regeneration of sinusoidal endothelial cells. *Cell Stem Cell* 4(3):263–274.
36. Gartner LP, Hiatt JL (1997) *Color Textbook of Histology* (Saunders, Philadelphia), 3rd Ed.
37. Koch CA, Li CY, Mesa RA, Tefferi A (2003) Nonhepatosplenic extramedullary hematopoiesis: Associated diseases, pathology, clinical course, and treatment. *Mayo Clin Proc* 78(10):1223–1233.
38. O'Malley DP (2007) Benign extramedullary myeloid proliferations. *Mod Pathol* 20(4): 405–415.
39. Miyata T, Masuzawa M, Katsuoka K, Higashihara M (2008) Cutaneous extramedullary hematopoiesis in a patient with idiopathic myelofibrosis. *J Dermatol* 35(7):456–461.
40. Lee J, Cuddihy MJ, Kotov NA (2008) Three-dimensional cell culture matrices: State of the art. *Tissue Eng Part B Rev* 14(1):61–86.
41. Fisher OZ, Khademhosseini A, Langer R, Peppas NA (2010) Bioinspired materials for controlling stem cell fate. *Acc Chem Res* 43(3):419–428.
42. Marshall AJ, et al. (2004) Biomaterials with tightly controlled pore size that promote vascular in-growth. *ACS Polymer Preprints* 45(2):100–101.
43. Jain RK, Munn LL, Fukumura D (2002) Dissecting tumour pathophysiology using intravital microscopy. *Nat Rev Cancer* 2(4):266–276.
44. Orth JD, et al. (2011) Analysis of mitosis and antimitotic drug responses in tumors by in vivo microscopy and single-cell pharmacodynamics. *Cancer Res* 71(13):4608–4616.
45. Roussos ET, et al. (2011) Mena invasive (MenaINV) promotes multicellular streaming motility and transendothelial migration in a mouse model of breast cancer. *J Cell Sci* 124(Pt 13):2120–2131.
46. Lo Celso C, Wu JW, Lin CP (2009) In vivo imaging of hematopoietic stem cells and their microenvironment. *J Biophotonics* 2(11):619–631.